Heterogeneity of vegetation structure interacts with fuel moisture to affect forest resistance to wildfire

Michael J Koontz[1] , Malcolm P North[2] , Stephen E Fick[3] , Chhaya M Werner[4] , Andrew M Latimer[5]

[1]Graduate Group in Ecology, University of California, Davis; Davis, CA
[2]Pacific Southwest Research Station, USDA Forest Service; Mammoth Lakes, CA
[3]USGS/University of Colorado, Boulder; Boulder, CO
[4]Center for Population Biology, University of California, Davis; Davis, CA
[5]Department of Plant Science, University of California, Davis; Davis, CA

Abstract. Variation in the size and distribution of trees can enable a forest to withstand ongoing disturbances and retain its essential identity and function. We test this phenomenon at a broad spatial extent in California's Sierra Nevada region using remotely-sensed data corroborated with on the ground measurements. We find that greater heterogeneity in local forest structure reduces the probability of a high severity wildfire in normal fuel moisture conditions, but increases the probability of high severity fire in extreme fuel moisture conditions. For a given local vegetation density, a more heterogeneous forest comprises a greater range of sparse and dense vegetation patches compared to a homogenous forest. We conclude that, under normal fuel moisture conditions, the effect of the sparse vegetation patches in a heterogeneous forest dominates– fire spread is interrupted and the probability of a high severity fire is reduced. Under extreme fuel moisture conditions, the effect of the dense vegetation patches in a heterogeneous forest dominates– those dense patches are more likely to burn at high severity and conditions are ripe for their high severity to be more contagious for nearby vegetation. Heterogeneous forest structure thus makes mixed conifer forest in the Sierra Nevada more resistant to this inevitable disturbance under most fuel moisture conditions, and may increase the probability of its long-term persistence. However, increasing fire activity driven by greater aridity resulting from anthropogenic global change may ultimately lead to more fires burning in extreme fuel moisture conditions in which heterogeneity will increase fire severity.

Introduction

Biological systems comprising heterogeneous elements can retain their fundamental properties in the face of regular disturbance. This ability of a heterogeneous system to absorb disturbances, reorganize, and to persist within a domain of stability with respect to its identity, structure, function, and feedbacks is termed resilience (Holling 1973; Gunderson 2000; Folke *et al.* 2004; Walker *et al.* 2004). Resilience has been demonstrated in complex biological systems characterized by a variety of different types of "heterogeneity" including genetic diversity (Reusch *et al.* 2005; Agashe 2009; Baskett *et al.* 2009), species diversity (Tilman 1994; Chesson 2000; Cadotte *et al.* 2013), functional diversity (Gazol & Camarero 2016), topoclimatic complexity (Ackerly *et al.* 2010, @Lenoir2013), and temporal environmental variation (Questad & Foster 2008). An emerging paradigm in forest ecology is that spatial heterogeneity in the structure of vegetation on the landscape can confer resilience to disturbances such as wildfire, drought, and insect outbreaks (Stephens *et al.* 2008;

North *et al.* 2009; Virah-Sawmy *et al.* 2009). In California, increasing temperature coupled with increasing drought frequency exacerbate water stress on treesduring "hotter droughts" (Park Williams *et al.* 2012; Millar & Stephenson 2015). Further, a century of fire suppression policy has led to drastic densification and homogenization of forest structure in the Sierra Nevada (North *et al.* 2015). Wildfire regimes have changed in these forests such that fires are bigger and burn more at higher severity (Miller & Thode 2007; Cansler & McKenzie 2014; Harvey *et al.* 2016). Changes in wildfire disturbance regimes are particularly suited to catalyze catastrophic shifts in ecosystems because of their feedback with spatial forest heterogeneity at multiple scales. Thus, western North American forests are experiencing novel, "unhealthy" conditions (*sensu* Raffa *et al.* (2009)) that are liable to upset the feedbacks between forest structure and pattern-forming ecological disturbances that historically stabilized the system and made it resilient (Raffa *et al.* 2008; Millar & Stephenson 2015). Forests are of high management priority (Hansen *et al.* 2013; Crowther *et al.* 2015; Millar & Stephenson 2015; Trumbore *et al.* 2015), thus it is critical to understand the mechanisms underlying the effect of spatial heterogeneity in forest structure on forest resilience. In order to unite resilience theory with empirical observations, it is imperative to move from metaphors to measurements.

Resilience of forest systems is fundamentally challenging to quantify because they comprise long-lived species, span large geographic extents, and are affected by disturbances at a very broad range of spatial scales. A key feature of resilience is resistance– how easy it is to change the system state (Walker *et al.* 2004). In mixed conifer forests of California's Sierra Nevada mountain range, wildfire disturbance is most frequently associated with landscape-scale changes in system state. Wildfire severity describes the magnitude of these changes, with "high severity" signifying a stand-replacing event. Thus, a resistant forest system should generally experience lower wildfire severity when a fire inevitably occurs.

Severity describes the effect of a wildfire on an ecosystem– often the amount of vegetation mortality (Sugihara & Barbour 2006). Wildfire severity can be measured by comparing pre- and post-fire satellite imagery for a specific area, but this usually requires considerable manual effort for image collation and processing, followed by calibration with field data (Miller & Thode 2007; Miller *et al.* 2009; De Santis *et al.* 2010; Cansler & McKenzie 2012; Veraverbeke & Hook 2013; Parks *et al.* 2014; Prichard & Kennedy 2014; Edwards *et al.* 2018; Fernández-García *et al.* 2018). Efforts to measure severity across broad spatial extents, such as the Monitoring Trends in Burn Severity project (Eidenshink *et al.* 2007), are unsuitably subjective for rigourous scientific analysis though they serve their intended management purpose admirably (Kolden *et al.* 2015). Automated efforts to remotely assess wildfire have arisen, but they tend to focus on more aggregate measures of wildfire such as whether an area burned or the probability that it burned rather than the severity of the burn (Bastarrika *et al.* (2011); Goodwin & Collett (2014); Boschetti *et al.* (2015); Hawbaker *et al.* (2017) but see Reilly *et al.* (2017)). Here, we present a method to automate the measurement of wildfire severity using minimal user inputs: a geometry of interest (a wildfire perimeter or a field plot location) and an alarm date (the date the fire began). This information is readily available in many fire-prone areas (such as California, via the Fire and Resource Assessment Program; http://frap.fire.ca.gov/projects/fire_data/fire_perimeters_index) or could potentially be derived using existing products (such as the Landsat Burned Area Essential Climate Variable product described in Hawbaker *et al.* (2017)). Further, the flexibility of this approach faciliates collaborative calibration with field-collected wildfire severity data.

Vegetation characteristics such as canopy density (Rouse *et al.* 1973; Young *et al.* 2017), moisture content (Asner *et al.* 2015), insect attack (Näsi *et al.* 2015), and even functional diversity (Asner *et al.* 2017) can be measured using remotely-sensed imagery. Texture analysis of imagery can quantify ecologically relevant environmental heterogeneity across broad spatial scales (Wood *et al.* 2012). Texture analysis was originally developed for image classification and computer vision, and it characterizes each pixel in an image by a summary of its neighboring pixels (Haralick *et al.* 1973; Conners *et al.* 1984). Ecologists have successfully used texture measurements to augment predictions of species richness (Huang *et al.* (2014); Stein *et al.* (2014); Tuanmu & Jetz (2015) but see Culbert *et al.* (2012)).

Creation and maintenance of spatial heterogeneity

Forest structure is defined by the size and distribution of trees on the landscape. Differences in tree crown heights characterize vertical structure, while differences in the rooting locations of trees characterizes horizontal structure (North *et al.* 2009). Competition for light, water, and other resources can yield aggregations of trees within favorable microsites or more widely spaced trees to ameliorate detrimental interactions (Clyatt *et al.* 2016). Demographic processes of dispersal, recruitment, and mortality affect forest structure by adding or subtracting whole trees. Reciprocally, the forest structure can also influence these pattern-forming processes such as when vegetation overstory alters microclimate or changes tree demographic rates (Larson & Churchill 2012; De Frenne *et al.* 2013; Ford *et al.* 2013). The stabilizing effects of these reciprocal processes in forests are hallmarks of a resilient system (Folke *et al.* 2004). In the Sierra Nevada range of California, one of the strongest feedbacks between forest structure and pattern-generating ecological process relate to wildfire, which affects hundreds of thousands to millions of hectares of forested area per year in the Sierra Nevada (Larson & Churchill 2012; Park Williams *et al.* 2012; Millar & Stephenson 2015).

Wildfire interacts dynamically with the forest structures (Westerling *et al.* 2006; Larson & Churchill 2012; Park Williams *et al.* 2012). Wildfire can affect the future forest structure by changing demographic rates of individual trees (e.g. increasing growth or germination via increasing light or nitrogen availability), but it's most lasting impact to forest structure is in the pattern of killed trees left in its wake (Larson & Churchill 2012). Wildfire behavior is inherently complex and is influenced by local weather, topography, and heterogeneous fuel conditions created by departures from the average fire return interval at any particular place (Sugihara & Barbour 2006; Collins & Stephens 2010). For instance, high tree density and presence of "ladder fuels" in the understory increase the probability of crown fire that kills a high proportion of trees (Stephens *et al.* 2008; North *et al.* 2009). A heterogeneous forest can largely avoid overstory tree mortality because a reduced amount of accumulated ladder fuel decreases its ability to get into the crown (where mortality is more likely to result), because wide spacing between tree clumps interrupts high severity fire spread across the landscape, and because tree clumps with fewer trees don't facilitate self-propagating fire behavior (Graham *et al.* 2004; Scholl & Taylor 2010). In forests with relatively intact fire regimes and heterogeneous stand conditions such as in the Jeffrey pine forests of the Sierra San Pedro Martir in Baja, California, there tends to be reduced vegetation mortality after wildfires compared to fire-suppressed forests (Stephens *et al.* 2008). Thus, forests with heterogeneous structure are predicted to persist in that state due to resistance to inevitable wildfire disturbance (Graham *et al.* 2004; Moritz *et al.* 2005; Stephens *et al.* 2008). However, it is unclear whether this is true at broad spatial extents, nor is it resolved at what scale heterogeneity in forest structure is meaningful for resilience (Kotliar & Wiens 1990).

We use a new remote sensing approach to calculate wildfire severity across broad spatial extents as well as image texture analysis to ask: does spatial variability in forest structure make California mixed conifer forests more resilient by reducing the severity of wildfires when they occur? Further, we ask whether this process is dependent upon topographic, fire weather, or other fuel conditions.

Methods

This work occurred in two phases. First, we developed a new approach to calculating wildfire severity across broad spatial and temporal scales and calibrated our measurements to those frome the field. We applied this approach to all known fire perimeters in the Sierra Nevada region between 1984 and 2016 as defined by the Fire and Resource Assessment Program (FRAP, http://frap.fire.ca.gov/projects/fire_data/fire_perimeters_index), which is the most comprehensive digital record of fire occurrence in California. Second, we used texture analysis of remotely-sensed imagery bounded by the perimeters in the FRAP database to develop a measure of vegetation heterogeneity and modeled how that heterogeneity affected wildfire severity, accounting for other key drivers of wildfire behavior.

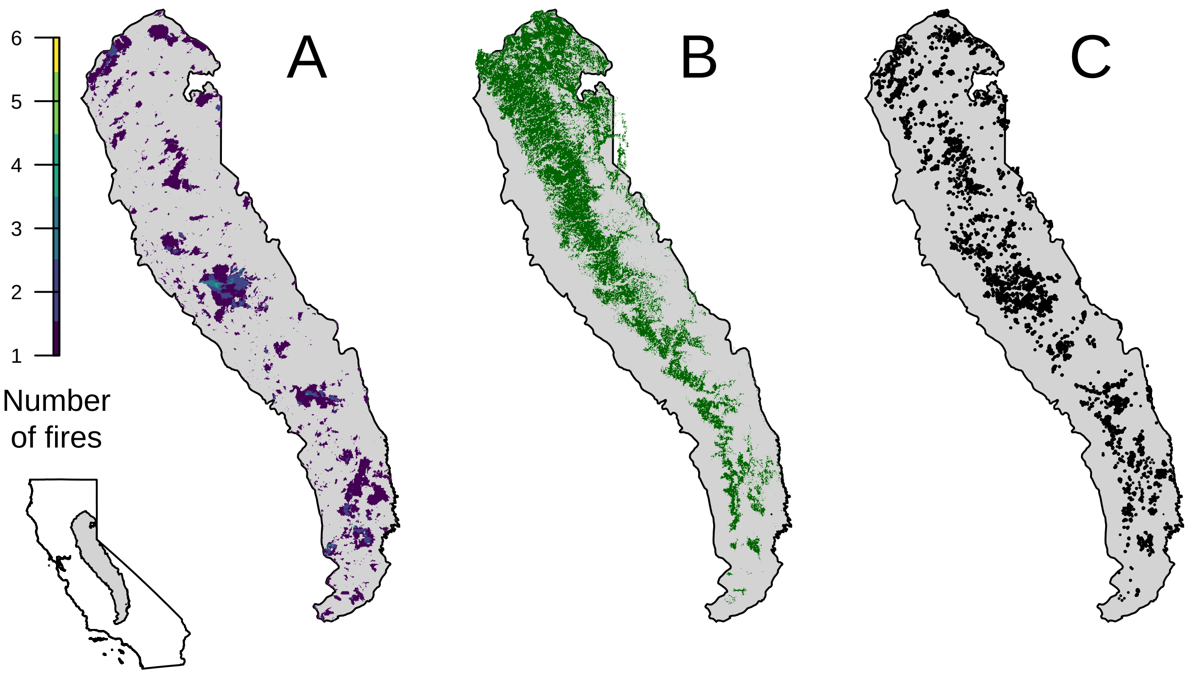

Figure 1: Geographic setting of the study. A) Locations of all fires that burned in yellow pine/mixed conifer forest between 1984 and 2016 in Sierra Nevada mountain range of California according to the State of California Fire Resource and Assessment Program database, the most comprehensive database of fire perimeters of its kind (data available for download from http://frap.fire.ca.gov/data/frapgisdata-sw-fireperimeters_download). Image represents a rasterized version of polygons from the FRAP database at a 100m x 100m pixel resolution. Colors indicate how many fire perimeters overlapped a given pixel within the study time period. B) Location of yellow pine/mixed conifer forests as designated by the Fire Return Interval Departure (FRID) product which, among other things, describes the potential vegetation in an area based on the pre-EuroAmerican colonization fire regime. (Data are available for download from https://www.fs.usda.gov/detail/r5/landmanagement/gis/?cid=STELPRDB5327836). Image represents a rasterized version of polygons from the FRID database at a 100m x 100m pixel resolution. C) Locations of random samples drawn from fires depicted in panel A that were in yellow pine/mixed conifer forest as depicted in panel B, and which were designated as "burned" by exceeding a threshold relative burn ratio (RBR) determined by calibrating the algorithm presented in this study with ground based composite burn index (CBI) measurements.

Study area

Our study assesses the effect of vegetation structure on wildfire severity in the Sierra Nevada mountain range of California in yellow pine/mixed conifer forests between 1984 and 2016. Forests in our study area are dominated by a mixture of conifer species including ponderosa pine (*Pinus ponderosa*), sugar pine (*Pinus lambertiana*), incense-cedar (*Calocedrus decurrens*), Douglas-fir (*Pseudotsuga menziesii*), white fir (*Abies concolor*), and red fir (*Abies magnifica*) (Stephens & Collins 2004; Collins *et al.* 2015). Tree density in the early 20th century was relatively low, with about 25-79 trees/ha and about 8-30 m2/ha of live basal area (Collins *et al.* 2015). Since this time, canopy cover has increased by 25-49%, overall tree density has increased by >75%, and white fir (*Abies concolor*) makes up a greater percentage of basal area compared to forests in the early 20th century (Stephens *et al.* 2015). The change in tree density is underlaid by a shift in size distribution: modern mixed conifer forests have 2.5 times as many trees between 30.4 and 61.0cm diameter at breast height (dbh) per hectare (103.9 versus 41.0 trees/ha) and half as many trees greater than 91.4cm dbh per hectare (8.7 versus 16.7 trees/ha) compared to forests in 1911 (Stephens *et al.* 2015).

Mixed conifer forests in the Sierra Nevada burned every 11 years on average for several centuries prior to Euro-American settlement (Steel *et al.* 2015). These relatively frequent burns prevented the accumulation of fuel on the ground, and limited the intensity of the next fire. This average fire return interval is short compared to the regeneration time of the dominant species, so the fire regime of Sierra Nevada mixed conifer forests in this period is usually classified as a "high frequency/low-mid severity" (Steel *et al.* 2015).

A new approach to remotely sensing wildfire severity

Wildfire severity can be reliably detected remotely by comparing pre- and postfire imagery from sensors aboard the Landsat series of satellites (Eidenshink *et al.* 2007; Miller & Thode 2007). The Thematic Mapper (TM; Landsat 4 and 5), Enhanced Thematic Mapper Plus (ETM+; Landsat 7), and Operational Land Imager (OLI; Landsat 8) sensors generate compatible top-of-atmosphere (TOA) spectral reflectance data suitable for scientific analysis. Recent advances in radiometric correction post-processing can compensate for various atmospheric distortions and generate more accurate measurements of surface reflectance in narrow wavelength bands spanning the electromagnetic spectrum (Masek *et al.* 2006; Vermote *et al.* 2016; USGS 2017b, a). Landsat satellites image the entire Earth approximately every 16-days and repeat images of the same area are geometrically coregistered such that overlapping pixels correspond to the same area on the ground. We used Google Earth Engine, a cloud-based geographic information system and image hosting platform, for all image collation and processing in order to leverage the centralized availability of the latest processed satellite images and integrated image processing tools for broad-scale analyses (Gorelick *et al.* 2017).

The base assumption of our new approach to calculating wildfire severity is that each fire's geographic data and associated attributes are represented by a self-contained "feature". Many fire datasets (e.g., FRAP, USFS Region 5 Fire Perimeter Data, CBI field plot locations from Zhu *et al.* (2006) and Sikkink *et al.* (2013)) already meet this criteria. In order to achieve a programmatic, automatic assessment of wildfire severity, severity-calculating algorithms must be able to use only the information within each feature. Time efficiencies and data compatibility benefits are attained when those algorithms are applied across an entire feature collection, performing their operation on each feature in turn. At a minimum, our algorithm requires that each feature contain some geographic information (e.g., a fire perimeter or a cbi plot location) and a fire start date (i.e., an "alarm date").

Fetching and processing pre- and postfire imagery

All Landsat imagery was fetched by "scene"– the atomic unit of image data in the Landsat collection representing an area on the Earth's surface approximately 170 km long by 183 km wide. For each feature, a collection of Landsat scenes was fetched both before and after the fire by defining a date range to search for imagery. The date range for prefire imagery started one day before each feature's alarm date and extended backward in time by a user-defined time window. The date range for postfire imagery was exactly one year after the date range for the prefire search (i.e., one year after the day before the fire, extending backward in time by the same time window). We tested 4 time windows: 16, 32, 48, or 64 days which were chosen to ensure that at least 1, 2, 3, or 4 Landsat images, taken on a 16-day interval, were captured by the date ranges (Fig. 2 2).

The Landsat archive was filtered to generate a prefire image collection comprising only the Landsat scenes depicting some part of the feature geometry and within the prefire date range. A postfire image collection was similarly generated by filtering the Landsat archive by the postfire date range and the feature geometry. The Landsat archive we filtered included imagery from Landsat 4, 5, 7, and 8, so each pre- and postfire image collection may contain a mix of scenes from different satellite sources to enhance coverage.

For each image in the pre- and postfire image collections, we masked pixels that were not clear (i.e., clouds, cloud shadows, snow, and water) and calculated standard indices that capture vegetation cover and fire effects such as charring: normalized difference vegetation index (NDVI; Eq. 1 1; Rouse *et al.* (1973)), normalized difference moisture index (NDMI; Eq. 2 2; Gao (1996)), normalized burn ratio (NBR; Eq. 3 3; Key & Benson (2006); USGS (2017a); USGS (2017b)), and normalized burn ratio version 2 (NBR2; Eq. 4 4; USGS (2017a);

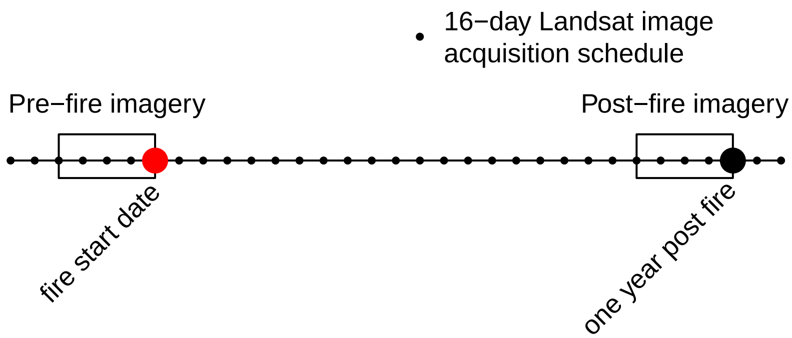

Figure 2: Schematic for how Landsat imagery was assembled in order to make comparisons between pre- and post-fire conditions. This schematic depicts a 64-day window of image collation prior to the fire which comprise the pre-fire image collection. A similar, 2-month window collection of imagery is assembled one year after the pre-fire image collection.

USGS (2017b); Hawbaker *et al.* (2017)).

(1)

$$ndvi = (nir - red)/(nir + red)$$

(2)

$$ndmi = (nir - swir1)/(nir + swir1)$$

(3)

$$nbr = (nir - swir2)/(nir + swir2)$$

(4)

$$nbr2 = (swir1 - swir2)/(swir1 + swir2)$$

Where nir is the near infrared band (band 4 on Landsat 4, 5, and 7; band 5 on Landsat 8) and red is the red band (band 3 on Landsat 4, 5, and 7; band 4 on Landsat 8), $swir1$ is the first short wave infrared band (band 5 on Landsat 4, 5, and 7; band 4 on Landsat 8), $swir2$ is the second short wave infrared band (band 7 on Landsat 4, 5, 7, and 8)

We summarized each prefire image collection into a single prefire image using a median reducer, which calculated the median of the unmasked values on a per-pixel basis across the stack of images in the prefire collection. We similarly summarized the postfire image collection into a single postfire image.

Calculating wildfire severity

We calculated remotely-sensed wildfire severity using the relative burn ratio (RBR) (Parks *et al.* 2014), the delta normalized burn ratio (dNBR) (Eidenshink *et al.* 2007; Miller & Thode 2007), the relative delta normalized burn ratio (RdNBR) (Miller & Thode 2007), the delta normalized burn ratio 2 (dNBR2) (Hawbaker *et al.* 2017), the relative delta normalized burn ratio 2 (RdNBR2), and the delta normalized difference vegetation index (dNDVI) (Eidenshink *et al.* 2007). Following the success of the RdNBR metric in other studies, we also calculate an analogous metric using NDVI– the relative delta normalized difference vegetation index (RdNDVI).

We calculated the delta severity indices (dNBR, dNBR2, dNDVI) by subracting the respective postfire indices from the prefire indices (NBR, NBR2, and NDVI) without multiplying by a rescaling constant (e.g., we did not multiply the result by 1000 as in Miller & Thode (2007); Eq. 5 5). Following Reilly *et al.* (2017), we chose not to correct the delta indices using a phenological offset value (typically calculated as the delta index in homogenous forest patch outside of the fire perimeter), as our approach implicitly accounts for phenology by incorporating multiple cloud-free images across the same time window both before the fire and one year later.

(5)

$$dI = I_{\text{prefire}} - I_{\text{postfire}}$$

We calculated the relative delta severity indices, RdNBR and RdNDVI, by scaling the respective delta indices (dNBR and dNDVI) from Eq. 5 6 by a square root transformation of the absolute value of the prefire index:

(6)

$$RdI = \frac{dI}{\sqrt{|I_{\text{prefire}}|}}$$

We calculated the relative burn ratio (RBR) following Parks *et al.* (2014):

(7)

$$RBR = \frac{dNBR}{NBR_{\text{prefire}} + 1.001}$$

Calibrating remotely-sensed wildfire severity with field-measured wildfire severity

We calibrated our remotely-sensed measure of wildfire severity with 208 field measures of overstory tree mortality from two previously published studies (Zhu *et al.* 2006; Sikkink *et al.* 2013) (Fig. 4 4). The Composite Burn Index (CBI) is a metric of change in vegetation across several vertical strata (Key & Benson

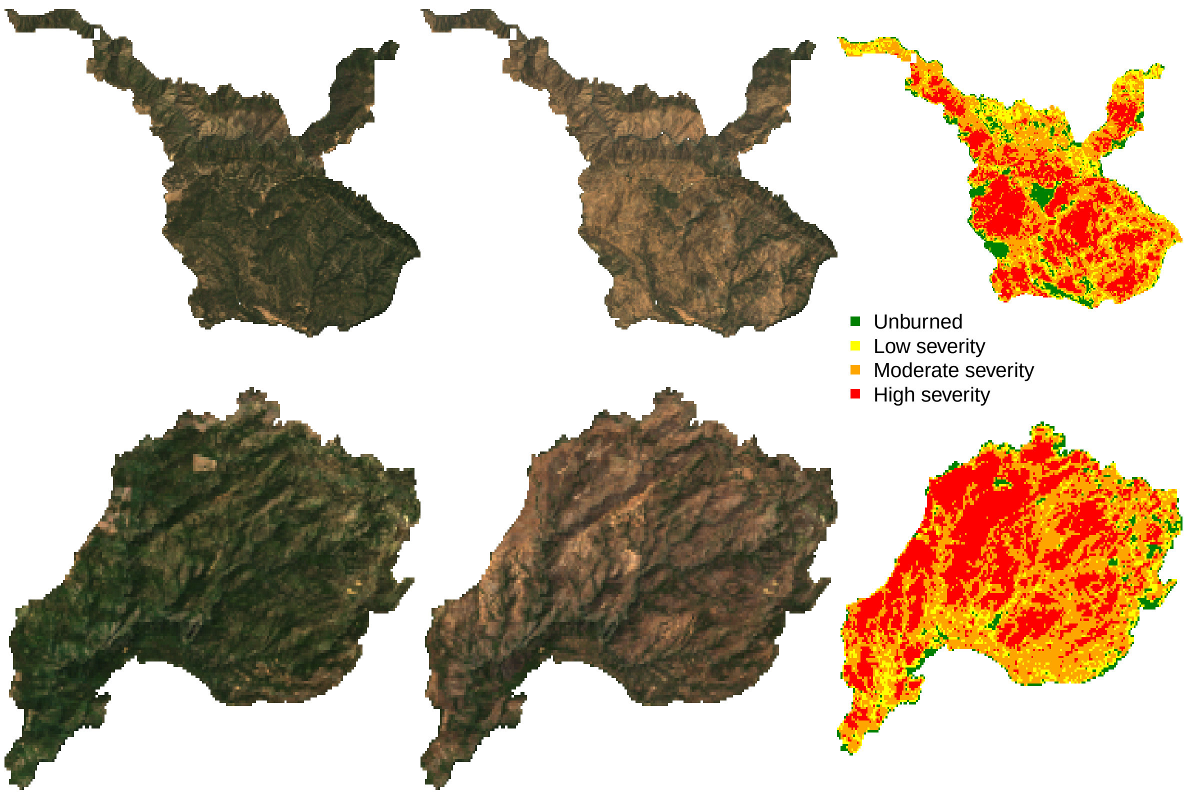

Figure 3: Example algorithm outputs for the Hamm Fire of 1987 (top row) and the American Fire of 2013 (bottom row) showing: prefire true color image (left column), postfire true color image (center column), relative burn ratio (RBR) calculation using a 48-day image collation window before the fire and one year later. For visualization purposes, these algorithm outputs have been resampled to a resolution of 100m x 100m from their original resolution of 30m x 30m. Data used for analyses were sampled from the outputs at the original resolution.

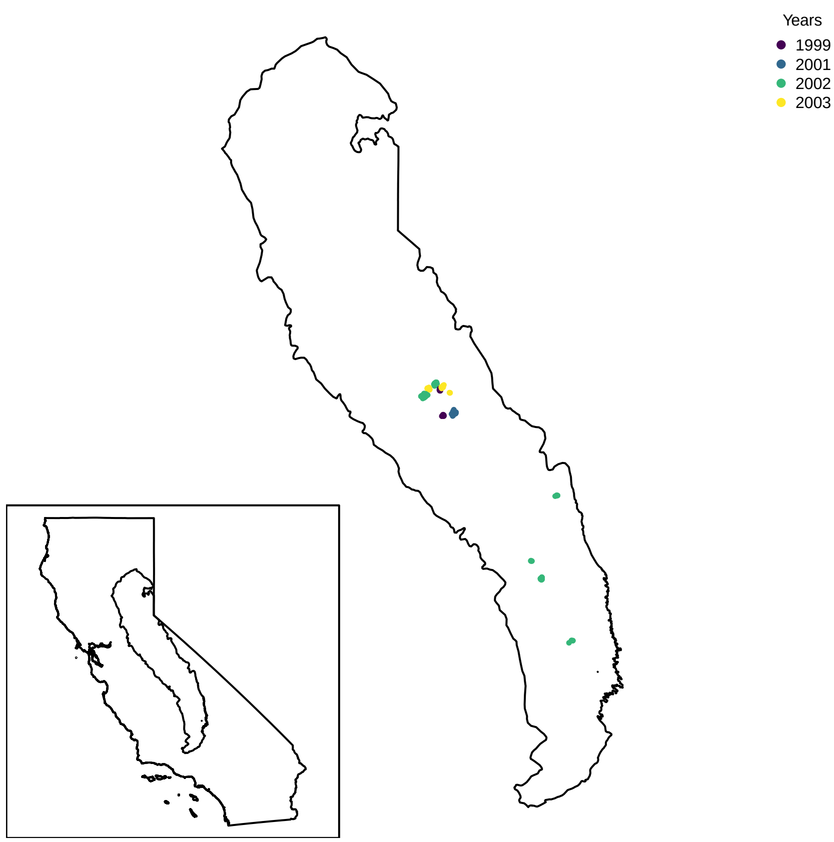

Figure 4: Location of CBI plots in the Sierra Nevada mountain range of California

2006) and has a long history of use in calibrating remotely-sensed severity data (Miller & Thode 2007; Miller *et al.* 2009; Cansler & McKenzie 2012; Parks *et al.* 2014; Prichard & Kennedy 2014). Following Miller & Thode (2007), Miller *et al.* (2009), and Parks *et al.* (2014), we fit a non-linear model to each remotely-sensed severity metric of the following form:

(8)

$$\text{remote\_severity} = \beta_0 + \beta_1 e^{\beta_2 \text{cbi\_overstory}}$$

We fit the model in Eq. 8 8 for all 7 of our remotely-sensed severity metrics (RBR, dNBR, RdNBR, dNBR2, RdNBR2, dNDVI, RdNDVI) using 4 different time windows from which to collate satellite imagery (16, 32, 48, and 64 days). Following Cansler & McKenzie (2012) and Parks *et al.* (2014), we used interpolation to extract remotely-sensed severity at the locations of the CBI field plots to better align remote and field measures of severity. We extracted remotely-sensed severity values using both bilinear interpolation, which returns a severity value weighted by the 9 pixel values nearest to the CBI plot location, and bicubic interpolation, which returns a severity value weighted by the 16 pixel values nearest to the CBI plot location. In total, we fit 56 models (7 severity measures, 4 time windows, 2 interpolation methods) and performed five-fold cross validation using the `modelr` and `purrr` packages. To compare goodness of model fits with Miller & Thode (2007), Miller *et al.* (2009), and Parks *et al.* (2014), we report the average R^2 value from the five folds for each of the 56 models but note that R^2 for non-linear regressions do not have the same interpretation that they do for linear regression (i.e., R^2 can be greater than 1 for non-linear regression, so it can't be interpreted as the proportion of variation explained by the model). We used the Relative Burn Ratio (RBR) calculated using bicubic interpolation within a 48-day window as our response variable for analyses of vegetation heterogeneity, as it showed the best correspondence to field severity data measured as average R^2 across the five folds.

Remote sensing other conditions

Heterogeneity of vegetation

We used texture analysis to calculate a first order, remotely-sensed measure of forest heterogeneity (Haralick *et al.* 1973; Tuanmu & Jetz 2015). Within a moving square neighborhood window with sides of 90m, 150m, 210m, and 270m (corresponding to a moving neighborhood window of 0.81 ha, 2.25 ha, 4.41 ha, and 7.29 ha), we calculated heterogeneity for each pixel as the standard deviation of the NDVI values of its neighbors (not including itself) (See Fig. 5 5).

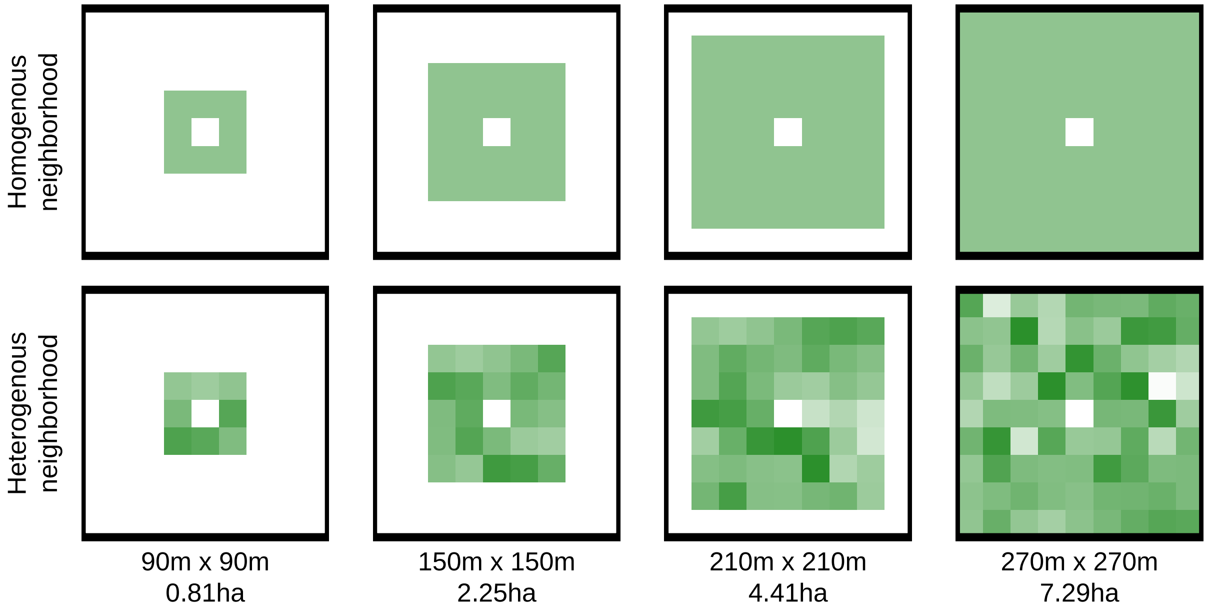

Figure 5: Example of homogenous forest (top row) and heterogenous forest (bottom row) with the same mean NDVI values (~0.6). Each column represents heterogeneity measured using a different neighborhood size.

Topographic conditions

Elevation data were sourced from the Shuttle Radar Topography Mission (Farr *et al.* 2007), a 1-arc second digital elevation model. Slope and aspect were extracted from the digital elevation model. Per-pixel topographic roughness was calculated as the standard deviation of elevation values within a the same kernel sizes as those used for vegetation heterogeneity (approximately 90m, 150m, 210m, and 270m on a side and not including the central pixel). Some work has shown that terrain ruggedness (Holden *et al.* 2009), and particularly coarser-scale terrain ruggedness (Dillon *et al.* 2011), is an important predictor of wildfire severity.

We used the digital elevation model to calculate the potential annual heat load (Eq. 9 9 at each pixel, which is an integrated measure of latitude, slope, and a folding transformation of aspect about the northeast-southwest line, such that northeast becomes 0 radians and southwest becomes π radians (McCune & Keon (2002) with correction in McCune (2007)):

(9)

$$
\begin{aligned}
aspect_{folded} &= |\pi - |aspect - \frac{5\pi}{4}|| \\
log(pahl) &= -1.467+ \\
&\quad 1.582 * cos(latitude)cos(slope)- \\
&\quad 1.5 * cos(aspect_{folded})sin(slope)sin(latitude)- \\
&\quad 0.262 * sin(lat)sin(slope)+ \\
&\quad 0.607 * sin(aspect_{folded})sin(slope)
\end{aligned}
$$

Where $pahl$ is the potential annual heat load, $aspect_{folded}$ is a transformation of aspect in radians, and both $latitude$ and $slope$ are extracted from a digital elevation model with units of radians.

Fire weather conditions

The 100-hour fuel moisture data were sourced from the Gridmet product (Abatzoglou 2013) and were calculated as the median 100-hour fuel moisture for the 3 days prior to the fire. We included a boolean variable for extreme values of 100-hour fuel moisture if they were lower than 7.7%, since these values fall below the 20$^{\text{th}}$ percentile of 100-hour fuel moisture for the Sierra Nevada region (Stephens *et al.* 2013).

Modeling the effect of heterogeneity on severity

We scaled all continuous predictor variables (keeping the boolean variable representing whether the fire weather was extreme or not unscaled), and treated each individual fire as having a random intercept effect using the following mixed effects logistic regression model:

(10)

$$
\begin{aligned}
severity_{i,j} &\sim Bern(\phi_{i,j}) \\
logit(\phi_{i,j}) &= \beta_0 + \\
&\quad \beta_{\text{heterogeneity}} * \text{heterogeneity}_i + \\
&\quad \beta_{\text{extreme\_fm100}} * \text{extreme\_fm100}_i + \\
&\quad \beta_{\text{fm100}} * \text{fm100}_i + \\
&\quad \beta_{\text{prefire\_ndvi}} * \text{prefire\_ndvi}_i + \\
&\quad \beta_{\text{topographic\_roughness}} * \text{topographic\_roughness}_i + \\
&\quad \beta_{\text{pahl}} * \text{pahl}_i + \\
&\quad \beta_{\text{heterogeneity*extreme\_fm100}} * \text{heterogeneity}_i * \text{extreme\_fm100}_i + \\
&\quad \beta_{\text{heterogeneity*fm100}} * \text{heterogeneity}_i * \text{fm100}_i + \\
&\quad \beta_{\text{extreme\_fm100*fm100}} * \text{extreme\_fm100}_i * \text{fm100}_i + \\
&\quad \beta_{\text{heterogeneity*extreme\_fm100*fm100}} * \text{heterogeneity}_i * \text{extreme\_fm100}_i * \text{fm100}_i + \\
&\quad \gamma_j \\
\gamma_j &\sim \mathcal{N}(0, \sigma_{\text{fire}})
\end{aligned}
$$

Each neighborhood size (90x90m, 150x150m, 210x210m, and 270x270m) was substituted in turn for the heterogeneity of NDVI, neighborhood mean NDVI, and terrain ruggedness covariates to generate a candidate set of 4 models.

To assess the effect of heterogeneity of forest structure on the probability of a high-severity wildfire, we contrasted two different combinations of the β coefficients: 1) a combination that corresponded to the effect of a one standard deviation increase in heterogeneity for a forested area in non-extreme fuel moisture conditions (extreme_fm100 = 0) with an average prefire NDVI (scaled \$prefire_ndvi = \$ 0), potential annual heat load (scaled \$pahl = \$ 0), and topographic roughness (scaled topographic_roughness = 0), as well as an average 100-hour fuel moisture for non-extreme fuel moisture conditions (\$fm100 = \$ 0.888), and 2) a combination that corresponded to the effect of a one standard deviation increase in heterogeneity for a forested area in extreme fuel moisture conditions (\$extreme_fm100 = \$ 1) with an average prefire NDVI (scaled \$prefire_ndvi = \$ 0), potential annual heat load (scaled \$pahl = \$ 0), and topographic roughness (scaled \$topographic_roughness = \$ 0), as well as an average 100-hour fuel moisture for extreme fuel moisture conditions (\$fm100 = \$ -0.588).

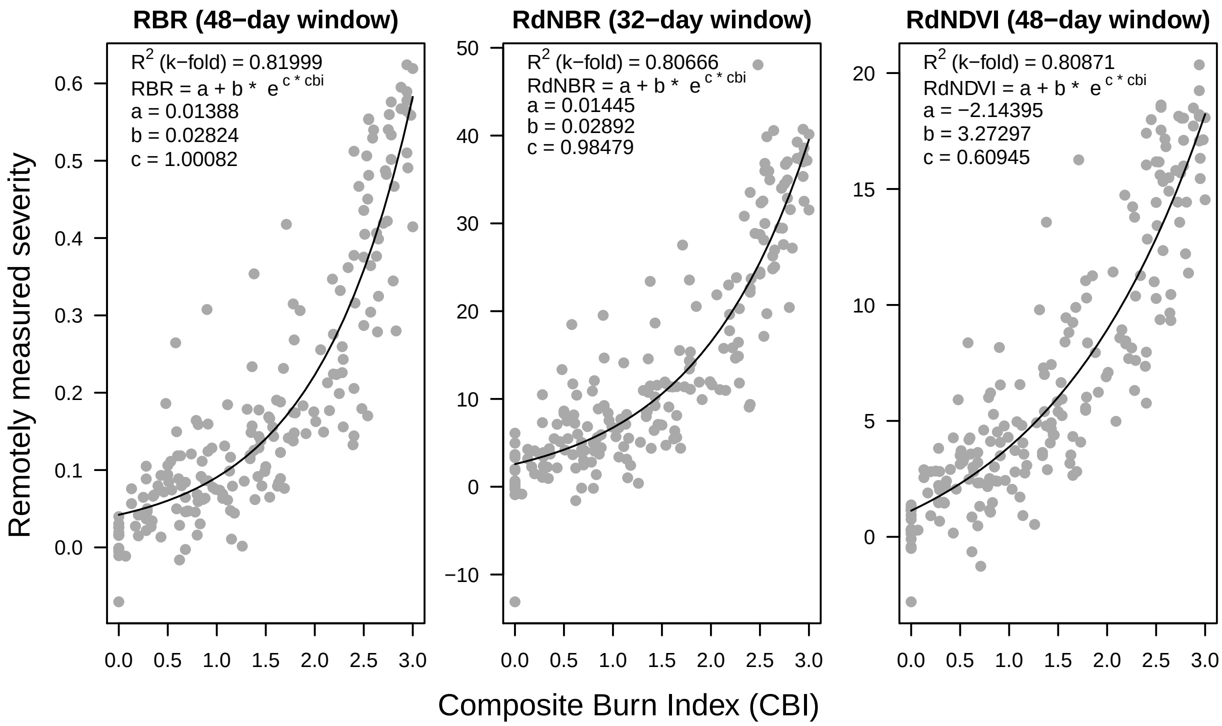

Figure 6: Calibration of three remotely-sensed severity metrics using new automated image collation algorithm to 208 field measures of severity.

Statistical software and data availability

We used `R` for all statistical analyses (R Core Team 2018). We used the `brms` package to fit mixed effects models (Bürkner 2017). We used a No U-Turn Sampler (NUTS) with 4 chains and 2000 samples per chain. Chain convergence was assessed for each estimated parameter by ensuring Rhat values were less than or equal to 1.01.

Data are available via the Open Science Framework.

Results

A new approach to remotely sensing wildfire severity

We found that the remotely sensed relative burn ratio (RBR) metric of wildfire severity measured across a 48 day interval prior to the wildfire alarm date correlated best with ground based composite burn index (CBI) measurements of severity (5-fold cross validation $Rˆ2 = $ 0.82; Table 1). Our method to calculate remotely sensed severity using automated Landsat image fetching performs as well or better than most other reported methods that use hand-curation of Landsat imagery (Edwards *et al.* 2018). Further, several combinations of remotely sensed severity metrics, time windows, and interpolation methods validate well with the ground based severity metrics, including those based on NDVI which is calculated using reflectance in shorter wavelengths than those typically used for measuring severity (Table 1). The top three models are depicted in Fig. 6 6.

Table 1: Comparison of models used to validate and calibrate remotely sensed wildfire severity with ground based composite burn index (CBI) severity sorted in descending order by the R^2 value from a 5-fold cross validation. A total of 56 models were tested representing all possible combinations of 7 different measures of wildfire severity (RBR, dNBR, dNBR2, RdNBR, RdNBR2, dNDVI, and RdNDVI), 4 different time windows in which Landsat imagery was acquired and summarized with a median reducer on a pixel-by-pixel basis (16 days, 32 days, 48 days, and 64 days), and two different interpolation methods (bilinear and bicubic). The three parameters (β_0, β_1, and β_2) from the nonlinear model fit described in Eq. 8 are reported. For each model, the value of the remotely sensed wildfire severity measurement corresponding to the lower bounds of 3 commonly used categories of severity are reported ('low' corresponds to a CBI value of 0.1, 'mod' corresponds to a CBI value of 1.25, and 'high' corresponds to a CBI value of 2.25)

Rank	Severity measure	Time window	Interpolation	k-fold R^2	β_0	β_1	β_2	low	mod	high
1	RBR	48	bicubic	0.820	0.014	0.028	1.001	0.045	0.113	0.282
2	RdNBR	32	bilinear	0.813	-0.483	3.061	0.857	2.852	8.450	20.559
3	RdNDVI	48	bilinear	0.809	-2.144	3.273	0.609	1.335	4.867	10.753
4	RBR	32	bilinear	0.807	0.014	0.029	0.985	0.046	0.113	0.280
5	RdNDVI	64	bicubic	0.805	-2.524	3.570	0.590	1.263	4.936	10.929
6	RBR	64	bicubic	0.805	0.016	0.027	1.010	0.046	0.113	0.283
7	RdNDVI	32	bicubic	0.803	-2.737	3.308	0.619	0.782	4.436	10.586
8	RBR	64	bilinear	0.802	0.017	0.027	1.003	0.047	0.113	0.279
9	RdNDVI	32	bilinear	0.801	-2.531	3.176	0.624	0.849	4.393	10.387
10	RdNDVI	48	bicubic	0.797	-2.623	3.624	0.587	1.220	4.922	10.943
11	RdNDVI	64	bilinear	0.796	-2.140	3.287	0.607	1.353	4.876	10.728
12	RdNBR	64	bilinear	0.792	-0.420	3.031	0.862	2.884	8.483	20.663
13	RBR	48	bilinear	0.791	0.017	0.027	1.006	0.047	0.112	0.277
14	RBR	32	bicubic	0.790	0.013	0.029	0.994	0.045	0.114	0.284
15	RdNBR	48	bicubic	0.785	-0.858	3.219	0.852	2.647	8.476	21.021
16	RBR	16	bilinear	0.781	0.021	0.026	1.016	0.050	0.114	0.278
17	RdNBR	32	bicubic	0.776	-0.954	3.340	0.841	2.679	8.602	21.199
18	dNDVI	32	bicubic	0.776	-0.058	0.073	0.650	0.020	0.106	0.257

Rank	Severity measure	Time window	Interpolation	k-fold R^2	β_0	β_1	β_2	low	mod	high
19	dNBR	48	bicubic	0.775	0.030	0.035	1.069	0.068	0.161	0.413
20	RdNBR	16	bilinear	0.774	0.279	2.518	0.909	3.037	8.119	19.727
21	dNDVI	32	bilinear	0.772	-0.053	0.070	0.656	0.022	0.105	0.252
22	dNDVI	48	bicubic	0.772	-0.055	0.081	0.613	0.031	0.119	0.267
23	dNBR	32	bilinear	0.770	0.029	0.036	1.048	0.069	0.163	0.410
24	RdNBR2	64	bicubic	0.766	2.102	0.416	1.240	2.572	4.059	8.861
25	dNBR	32	bicubic	0.764	0.028	0.036	1.057	0.068	0.163	0.417
26	dNDVI	48	bilinear	0.762	-0.044	0.073	0.637	0.034	0.118	0.262
27	RBR	16	bicubic	0.761	0.021	0.026	1.028	0.049	0.114	0.281
28	dNBR	16	bilinear	0.760	0.033	0.036	1.048	0.073	0.167	0.417
29	RdNBR2	32	bilinear	0.759	1.435	0.625	1.100	2.132	3.906	8.861
30	RdNBR	16	bicubic	0.758	0.370	2.446	0.926	3.053	8.149	19.999
31	RdNBR2	32	bicubic	0.754	1.426	0.601	1.125	2.098	3.876	8.975
32	dNBR	64	bicubic	0.753	0.033	0.033	1.086	0.070	0.161	0.413
33	dNBR	64	bilinear	0.751	0.035	0.033	1.080	0.071	0.161	0.406
34	RdNBR2	48	bicubic	0.751	1.835	0.460	1.209	2.354	3.919	8.818
35	dNBR	48	bilinear	0.748	0.035	0.033	1.076	0.071	0.161	0.405
36	RdNDVI	16	bilinear	0.747	-0.983	2.503	0.678	1.695	4.856	10.515
37	dNDVI	64	bicubic	0.746	-0.055	0.082	0.609	0.032	0.120	0.266
38	dNDVI	64	bilinear	0.741	-0.046	0.075	0.627	0.034	0.118	0.261
39	RdNBR2	48	bilinear	0.737	1.802	0.497	1.174	2.361	3.956	8.766
40	RdNBR	64	bicubic	0.737	-1.448	3.651	0.819	2.515	8.717	21.611
41	RdNBR2	64	bilinear	0.735	2.027	0.451	1.204	2.536	4.060	8.801
42	dNBR	16	bicubic	0.729	0.032	0.036	1.058	0.072	0.168	0.423
43	dNBR2	32	bilinear	0.727	0.026	0.009	1.149	0.035	0.062	0.140
44	dNDVI	16	bicubic	0.726	-0.030	0.065	0.674	0.040	0.121	0.267
45	RdNDVI	16	bicubic	0.725	-1.248	2.681	0.665	1.618	4.908	10.721
46	dNBR2	32	bicubic	0.715	0.025	0.008	1.177	0.035	0.061	0.142
47	dNBR2	64	bilinear	0.714	0.036	0.006	1.283	0.043	0.064	0.137
48	dNDVI	16	bilinear	0.707	-0.023	0.060	0.689	0.042	0.120	0.261

Rank	Severity measure	Time window	Interpolation	k-fold R^2	β_0	β_1	β_2	low	mod	high
49	dNBR2	48	bilinear	0.686	0.033	0.006	1.248	0.040	0.063	0.137
50	RdNBR2	16	bilinear	0.682	1.928	0.465	1.189	2.452	3.983	8.676
51	dNBR2	16	bilinear	0.662	0.030	0.009	1.138	0.040	0.066	0.143
52	RdNBR2	16	bicubic	0.654	1.871	0.467	1.198	2.398	3.960	8.792
53	dNBR2	16	bicubic	0.635	0.029	0.009	1.156	0.039	0.066	0.145
54	RdNBR	48	bilinear	0.630	-3.445	5.132	0.724	2.072	9.235	22.700
55	dNBR2	48	bicubic	0.000	0.033	0.006	1.284	0.040	0.062	0.138
56	dNBR2	64	bicubic	0.000	0.037	0.005	1.313	0.043	0.064	0.139

Based on these model comparisons, we used the relative burn ratio (RBR) calculated using a 48-day time window before the fire and bicubic interpolation as our metric of severity. We created the boolean response variable representing whether the sampled point burned at high severity or not by determining whether the RBR exceeded 0.282, the threshold for high severity derived using the non-linear relationship in Eq. 8 8 (Table 1 1).

Prefire vegetation density, annual heat load, and topographic roughness effects on wildfire severity

We found that the strongest influence on the probability of a forested area burning at high severity is the density of the vegetation, as measured by the prefire NDVI ($\beta_{\text{prefire\_ndvi}} = 0.91$ (1 pixel radius; 95% CI = [0.842, 0.979]), 0.927 (2 pixel radius; 95% CI = [0.858, 0.994]), 0.94 (3 pixel radius; 95% CI = [0.872, 1.01]), 0.945 (4 pixel radius; 95% CI = [0.874, 1.012]) on the log-odds scale; Fig. 7 7). For all 4 models using different neighborhood sizes for the heterogeneity and topographic roughness predictors, a greater prefire NDVI led to a greater probability of high severity fire. Potential annual heat load, which integrates aspect, slope, and latitude, also had a strong positive relationship with the probability of a high severity fire ($\beta_{\text{pahl}} = 0.242$ (1 pixel radius; 95% CI = [0.195, 0.286]), 0.243 (2 pixel radius; 95% CI = [0.199, 0.288]), 0.243 (3 pixel radius; 95% CI = [0.198, 0.288]), 0.243 (4 pixel radius; 95% CI = [0.198, 0.288]); Fig. 7 7). Areas that were located on southwest facing slopes at lower latitudes tended to be more likely to burn at high severity. We found no effect of local topographic roughness on wildfire severity at any neighborhood size ($\beta_{\text{topographic\_roughness}} =$ -0.015 (1 pixel radius; 95% CI = [-0.06, 0.031]), -0.01 (2 pixel radius; 95% CI = [-0.058, 0.037]), -0.014 (3

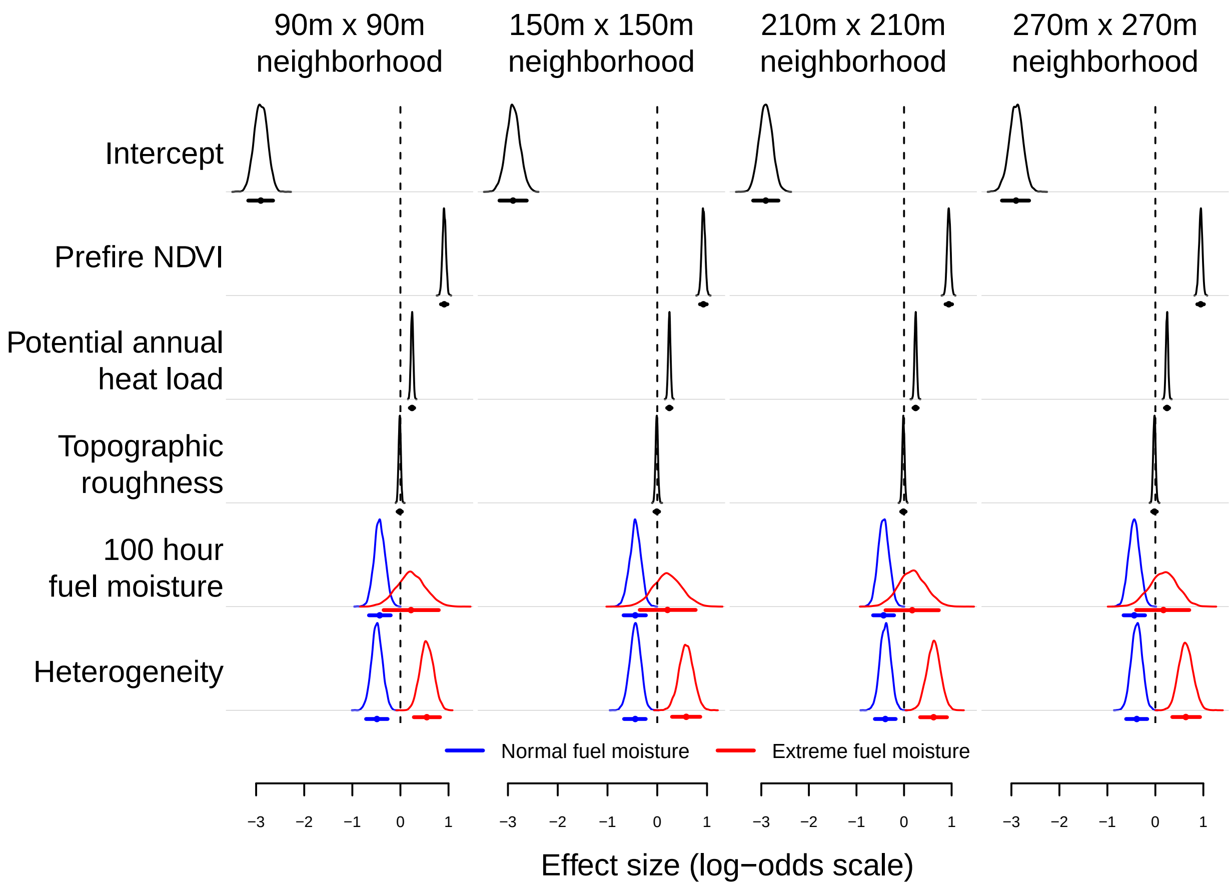

Figure 7: Half eye plots depicting the effect sizes for parameters of interest. Each column represents model results using a different neighborhood window size. Dot-whiskers along the x dimension represent mean and 95% credible intervals (using a symmetric quantile method) of each parameter of interest. The half eyes represent the posterior distributions of the parameters of interest. To depict interactions with whether the pixel burned under normal conditions (20th percentile or greater 100 hour fuel moisture) or extreme conditions (less than 20th percentile 100 hour fuel moisture), we show separate dot-whiskers and half eyes for the parameters that interact with the boolean “extreme conditions or not” variable. Blue lines represent parameter estimates under normal 100 hour fuel moisture conditions and red lines represent parameter estimates under extreme 100 hour fuel moisture conditions. For the effect of heterogeneity, the parameter estimates depicted represent the effect at the average fuel moisture value (on a standardized scale) in each condition. Thus, while other variables (e.g., potential annual heat load) are 0 in the calculation of the heterogeneity effect sizes to reflect the effect of heterogeneity at average values of those variables, the 100 hour fuel moisture variable is set to greater than 0 for normal conditions (to reflect that the average fuel moisture in normal conditions is higher than the overall average) and less than 0 for extreme conditions (to reflect that the average fuel moisture in extreme conditions is lower than the overall average).

pixel radius; 95% CI = [-0.061, 0.034]), -0.019 (4 pixel radius; 95% CI = [-0.068, 0.031]); Fig. 7 7).

100 hour fuel moisture effect on wildfire severity

We found a non-linear effect of 100 hour fuel moisture on wildfire severity such that, under normal fuel moisture conditions (100 hour fuel moisture greater than 20$^{\text{th}}$ percentile), increasing fuel moisture had a strong negative effect of the probability of a high severity wildfire (β_{fm100} = -0.432 (1 pixel radius; 95% CI = [-0.654, -0.202]), -0.442 (2 pixel radius; 95% CI = [-0.677, -0.228]), -0.43 (3 pixel radius; 95% CI = [-0.651, -0.209]), -0.441 (4 pixel radius; 95% CI = [-0.663, -0.215]); Fig. 7 7). However, under extreme fuel moisture conditions (100 hour fuel moisture less than 20$^{\text{th}}$ percentile), we detected no influence of fuel moisture on the probability of a high severity wildfire ($\beta_{\text{fm100}} + \beta_{\text{extreme\_fm100}} + \beta_{\text{extreme\_fm100*fm100}} = 0.22$ (1 pixel radius; 95% CI = [-0.349, 0.798]), 0.206 (2 pixel radius; 95% CI = [-0.352, 0.771]), 0.172 (3 pixel radius; 95% CI = [-0.39, 0.732]), 0.168 (4 pixel radius; 95% CI = [-0.401, 0.707]); Fig. 7 7).

Heterogeneity in vegetation structure effect on wildfire severity

We found strong evidence for an effect of heterogeneity of vegetation structure on the probability of a high severity wildfire. The effect was modulated by the fuel moisture conditions. Under normal fuel moisture conditions, an increasing heterogeneity of vegetation structure greatly reduced the probability of a high severity wildfire accounting for other variables ($\beta_{\text{heterogeneity}} + 0.888 * \beta_{\text{fm100}} + 0.888 * \beta_{\text{heterogeneity*fm100}} =$ -0.488 (1 pixel radius; 95% CI = [-0.714, -0.267]), -0.443 (2 pixel radius; 95% CI = [-0.667, -0.232]), -0.393 (3 pixel radius; 95% CI = [-0.613, -0.176]), -0.388 (4 pixel radius; 95% CI = [-0.609, -0.169])). This effect is nearly half as strong (but opposite in direction) as the dominant control on the mean probability of a high severity fire– the vegetation density (Fig. 7 7).

However, under extreme fuel moisture conditions, we found the opposite pattern: increasing heterogeneity of vegetation structure greatly *increased* the probability of a high severity wildfire, accounting for other variables ($\beta_{\text{heterogeneity}} + \beta_{\text{extreme\_fm100}} + -0.588 * \beta_{\text{fm100}} + \beta_{\text{heterogeneity*extreme\_fm100}} + -0.588 * \beta_{\text{heterogeneity*fm100}} + -0.588 * \beta_{\text{extreme\_fm100*fm100}} + -0.588 * \beta_{\text{heterogeneity*extreme\_fm100*fm100}} = 0.548$ (1 pixel radius; 95% CI = [0.279, 0.824]), 0.582 (2 pixel radius; 95% CI = [0.297, 0.864]), 0.621 (3 pixel radius; 95% CI = [0.337, 0.902]), 0.635 (4 pixel radius; 95% CI = [0.353, 0.931])). The effect size of heterogeneity in extreme conditions is half to nearly two-thirds the effect size of prefire vegetation density, and in the same positive direction (Fig. 7 7).

Discussion

We developed a new approach to calculating wildfire severity using remotely sensed images from the Landsat series of satellites using a minimal amount of user input– a geometry (i.e., a point location or a perimeter polygon) and a fire start date. We found that the relative burn ratio (RBR) calculated using prefire Landsat images collected over a 48 day period prior to the fire and postfire Landsat images collected over a 48 day period one year after the prefire images validated the best with ground based severity measurements (composite burn index; CBI). We also found that several other remotely sensed measures of severity validated nearly as well with CBI data.

We echo the conclusion of Zhu *et al.* (2006) that the validation of differences between pre- and postfire NDVI to field measured severity data, which uses near infrared reflectance, is comparable to validation using more commonly used severity metrics (e.g., RdNBR and dNBR) that rely on short wave infrared reflectance. One immediately operational implication of this is that the increasing availability of low-cost small unhumanned aerial systems (sUAS a.k.a. drones) and near infrared detecting imagers (e.g., those used for agriculture monitoring) may be used to measure wildfire severity at very high spatial resolutions.

We used our new approach to calculate wildfire severity for 920 fires that burned in the Sierra Nevada yellow pine/mixed conifer forest between 1984 and 2016. We additionally calculated 100 hour fuel moisture, local topographic roughness, potential annual heat load, prefire vegetation density, and the local heterogeneity of prefire vegetation density at 4 neighborhood sizes ranging from 0.81 hectares to 7.29 hectares. We modeled the effect of these variables on wildfire severity and found a strong positive relationship with both prefire vegetation density and potential annual heat load. We found no effect of topographic roughness on wildfire severity. We found a negative effect of 100 hour fuel moisture on severity, but only during normal fuel moisture conditions (100 hour fuel moisture greater than 20^{th} percentile). We found a strong negative effect of heterogeneity of vegetation structure on wildfire severity in normal fuel moisture conditions, and a strong positive effect of heterogeneity on severity in extreme fuel moisture conditions.

For similar vegetation density in a given local neighborhood, greater heterogeneity implies more of a mixture of dense patches and sparsely vegetated patches (see Fig. 5 5). Under non-extreme fuel moisture conditions, the more sparsely vegetation patches interrupt fuel continuity and reduce the likelihood of high severity fire. Under extreme fuel moisture conditions however, the more densely vegetated patches are more likely to burn at high severity and that high severity is more likley to be contagious.

Days with extreme fuel moisture conditions are likely to increase in a warming world (Abatzoglou & Williams 2016; Westerling 2016). This could have dire consequences for the formerly self-stabilizing heterogeneous forest/infrequent high severity fire system. Densification of forests as a result of fire suppression was always a problem with respect to increases in extreme fire behavior (large fires, more high severity). Coupled with anthropogenic global warming, we may have also broken our last forest structure tool for reducing wildfire severity– heterogeneity in structure.

Caveats

Our method should work best in denser vegetation such as forests, as the signal of a wildfire in other systems can be invisible in a matter of weeks (Goodwin & Collett 2014). This method would also require calibration with field data in other systems, as some severity metrics (such as RBR and RdNBR) have found limited success in other regions (Fernández-García *et al.* 2018).

We have captured a coarse measure of heterogeneity. While we did find that this coarse measure does strongly relate to fire severity, it does not account for fire behavior or spatial pattern forming processes at the individual tree scale. This may still be possible using remotely sensed data at a finer spatial resolution, but with a cost in temporal resolution and time series depth (e.g. NAIP imagery at 1m resolution but with only 3 total images starting in 2008) (Dickinson *et al.* 2016). Additional metrics of heterogeneity such as vegetation patch size distributions or non-vegetated gap size distributions (Malone *et al.* 2018), may also be more tractable using the finer spatial resolution of NAIP imagery.

Translating resistance to long term persistance

Texture analysis has been used to measure habitat heterogeneity in ecology, but has only recently gained recognition for its potential to quantify system resilience (Kéfi *et al.* 2014). For instance, increases in the second angular momentum of the configuration of vegetation patches may represent early warning signs of a catastrophic shift in a system whereby it converts to a vegetation-less desert. The change in this particular texture serves as an indicator of system precariousness because it reflects the spatial process by which the system stabilizes. In the case of desertification as a result of increasing grazing pressure, facilitation is the process driving vegetation patch configurations and the increase in spatial variation of those configurations indicates a breakdown in the process itself as the system moves nearer to a bifurcation point between a vegetated and a non-vegetated state. In our case, we measure heterogeneity as a spatial feature that is part of the feedback loop between disturbance and forest spatial structure, so we gain insight into longer-term patterns by measuring a signature of the pattern forming process itself. More work is needed to verify the degree to which the spatial features of mixed conifer forests– or the spatial features of the disturbances that affect them– capture the

Conclusions

We encourage researchers and managers to make their ground based severity data available with site location (including datum) and the alarm data for the fire the field data is measuring. Cloud-based GIS, central image hosting, and integration with powerful classification tools are sure to advance our ability to measure wildfire severity remotely, automatically, consistently, and at broad spatial scales. While our contribution here demonstrates that satisfactory validation with ground based measurements is possible using simple and well known calculations, we believe that truly groundbreaking abilities to classify wildfire severity would be possible with more open data sharing of ground based severity measures.

While the severity of a wildfire in any given place may be idiosyncratic and controlled by many variables, it is clear that heterogeneous forest structure generally makes mixed conifer forest in the Sierra Nevada more resistant to this inevitable disturbance under normal fuel moisture conditions. Because a resistant forest is a resilient forest, heterogeneity in forest structure may increase the probability of long-term forest persistence. Given the opposite effect of heterogeneity in extreme fuel moisture conditions and the normalization of what were once considered extreme fuel moisture conditions in a warming world,

1.

Abatzoglou, J.T. (2013). Development of gridded surface meteorological data for ecological applications and modelling. *International Journal of Climatology*, 33, 121–131.

2.

Abatzoglou, J.T. & Williams, A.P. (2016). The impact of anthropogenic climate change on wildfire across western US forests. *Proceedings of the National Academy of Sciences*, In press.

3.

Ackerly, D.D., Loarie, S.R., Cornwell, W.K., Weiss, S.B., Hamilton, H. & Branciforte, R. *et al.* (2010). The geography of climate change: Implications for conservation biogeography. *Diversity and Distributions*, 16, 476–487.

4.

Agashe, D. (2009). The stabilizing effect of intraspecific genetic variation on population dynamics in novel and ancestral habitats. *The American Naturalist*, 174, 255–67.

5.

Asner, G.P., Brodrick, P.G., Anderson, C.B., Vaughn, N., Knapp, D.E. & Martin, R.E. (2015). Progressive forest canopy water loss during the 2012–2015 California drought. *Proceedings of the National Academy of Sciences*, 2015, 201523397.

6.

Asner, G.P., Martin, R.E., Knapp, D.E., Tupayachi, R., Anderson, C.B. & Sinca, F. *et al.* (2017). Airborne laser-guided imaging spectroscopy to map forest trait diversity and guide conservation. *Science*, 355, 385–389.

7.

Baskett, M.L., Gaines, S.D. & Nisbet, R.M. (2009). Symbiont diversity may help coral reefs survive moderate climate change. *Ecological Applications*, 19, 3–17.

8.

Bastarrika, A., Chuvieco, E. & Martín, M.P. (2011). Mapping burned areas from landsat TM/ETM+ data with a two-phase algorithm: Balancing omission and commission errors. *Remote Sensing of Environment*, 115, 1003–1012.

9.

Boschetti, L., Roy, D.P., Justice, C.O. & Humber, M.L. (2015). MODIS-Landsat fusion for large area 30m burned area mapping. *Remote Sensing of Environment*, 161, 27–42.

10.

Bürkner, P.-C. (2017). brms : An R Package for Bayesian Multilevel Models Using Stan. *Journal of Statistical Software*, 80.

11.

Cadotte, M., Albert, C.H. & Walker, S.C. (2013). The ecology of differences: Assessing community assembly with trait and evolutionary distances. *Ecology Letters*, 16, 1234–1244.

12.

Cansler, C.A. & McKenzie, D. (2012). How robust are burn severity indices when applied in a new region? Evaluation of alternate field-based and remote-sensing methods. *Remote Sensing*, 4, 456–483.

13.

Cansler, C.A. & McKenzie, D. (2014). Climate, fire size, and biophysical setting control fire severity and spatial pattern in the northern Cascade Range, USA. *Ecological Applications*, 24, 1037–1056.

14.

Chesson, P. (2000). Mechanisms of maintenance of species diversity. *Annual Review of Ecology and Systematics*, 31, 343–366.

15.

Clyatt, K.A., Crotteau, J.S., Schaedel, M.S., Wiggins, H.L., Kelley, H. & Churchill, D.J. *et al.* (2016). Historical spatial patterns and contemporary tree mortality in dry mixed-conifer forests. *Forest Ecology and Management*, 361, 23–37.

16.

Collins, B.M., Lydersen, J.M., Everett, R.G., Fry, D.L. & Stephens, S.L. (2015). Novel characterization of landscape-level variability in historical vegetation structure. *Ecological Applications*, 25, 1167–1174.

17.

Collins, B.M. & Stephens, S.L. (2010). Stand-replacing patches within a 'mixed severity' fire regime: Quantitative characterization using recent fires in a long-established natural fire area. *Landscape Ecology*, 25, 927–939.

18.

Conners, R.W., Trivedi, M.M. & Harlow, C.A. (1984). Segmentation of a high-resolution urban scene using texture operators. *Computer Vision, Graphics, and Image Processing*, 25, 273–310.

19.

Crowther, T.W., Glick, H.B., Covey, K.R., Bettigole, C., Maynard, D.S. & Thomas, S.M. *et al.* (2015). Mapping tree density at a global scale. *Nature*, 525, 201–205.

20.

Culbert, P.D., Radeloff, V.C., St-Louis, V., Flather, C.H., Rittenhouse, C.D. & Albright, T.P. *et al.* (2012). Modeling broad-scale patterns of avian species richness across the Midwestern United States with measures of satellite image texture. *Remote Sensing of Environment*, 118, 140–150.

21.

De Frenne, P., Rodríguez-Sánchez, F., Coomes, D.A., Baeten, L., Verstraeten, G. & Vellend, M. *et al.* (2013). Microclimate moderates plant responses to macroclimate warming. *Proceedings of the National Academy of Sciences of the United States of America*, 110, 18561–5.

22.

De Santis, A., Asner, G.P., Vaughan, P.J. & Knapp, D.E. (2010). Mapping burn severity and burning efficiency in California using simulation models and Landsat imagery. *Remote Sensing of Environment*, 114, 1535–1545.

23.

Dickinson, Y., Pelz, K., Giles, E. & Howie, J. (2016). Have we been successful? Monitoring horizontal forest complexity for forest restoration projects. *Restoration Ecology*, 24, 8–17.

24.

Dillon, G.K., Holden, Z.A., Morgan, P., Crimmins, M.A., Heyerdahl, E.K. & Luce, C.H. (2011). Both topography and climate affected forest and woodland burn severity in two regions of the western US, 1984 to 2006. *Ecosphere*, 2, art130.

25.

Edwards, A.C., Russell-Smith, J. & Maier, S.W. (2018). A comparison and validation of satellite-derived fire severity mapping techniques in fire prone north Australian savannas: Extreme fires and tree stem mortality. *Remote Sensing of Environment*, 206, 287–299.

26.

Eidenshink, J., Schwind, B., Brewer, K., Zhu, Z.-l., Quayle, B. & Howard, S. (2007). A project for monitoring trends in burn severity. *Fire Ecology*, 3, 3–21.

27.

Farr, T., Rosen, P., Caro, E., Crippen, R., Duren, R. & Hensley, S. *et al.* (2007). The shuttle radar topography mission. *Reviews of Geophysics*, 45, 1–33.

28.

Fernández-García, V., Santamarta, M., Fernández-Manso, A., Quintano, C., Marcos, E. & Calvo, L. (2018). Burn severity metrics in fire-prone pine ecosystems along a climatic gradient using Landsat imagery. *Remote Sensing of Environment*, 206, 205–217.

29.

Folke, C., Carpenter, S., Walker, B., Scheffer, M., Elmqvist, T. & Gunderson, L. *et al.* (2004). Regime shifts, resilience, and biodiversity in ecosystem management. *Annual Review of Ecology, Evolution, and Systematics*, 35, 557–581.

30.

Ford, K.R., Ettinger, A.K., Lundquist, J.D., Raleigh, M.S. & Hille Ris Lambers, J. (2013). Spatial heterogeneity in ecologically important climate variables at coarse and fine scales in a high-snow mountain landscape. *PLoS ONE*, 8, e65008.

31.

Gao, B.C. (1996). NDWI - A normalized difference water index for remote sensing of vegetation liquid water from space. *Remote Sensing of Environment*, 58, 257–266.

32.

Gazol, A. & Camarero, J.J. (2016). Functional diversity enhances silver fir growth resilience to an extreme drought. *Journal of Ecology*.

33.

Goodwin, N.R. & Collett, L.J. (2014). Development of an automated method for mapping fire history captured in Landsat TM and ETM+ time series across Queensland, Australia. *Remote Sensing of Environment*, 148, 206–221.

34.

Gorelick, N., Hancher, M., Dixon, M., Ilyushchenko, S., Thau, D. & Moore, R. (2017). Remote Sensing of Environment Google Earth Engine : Planetary-scale geospatial analysis for everyone. *Remote Sensing of Environment*, 202, 18–27.

35.

Graham, R.T., McCaffrey, S. & Jain, T.B. (2004). *Science basis for changing forest structure to modify wildfire behavior and severity* (No. April). US Department of Agriculture, Forest Service, Rokcy Mountain Research Station, Fort Collins, CO.

36.

Gunderson, L.H. (2000). Ecological resilience– in theory and application. *Annual Review of Ecology and Systematics*, 31, 425–439.

37.

Hansen, M.C., Potapov, P.V., Moore, R., Hancher, M., Turubanova, S.A. & Tyukavina, A. (2013). High-resolution global maps of 21st-century forest cover change. *Science*, 342, 850–853.

38.

Haralick, R.M., Shanmugam, K. & Dinstein, I. (1973). Textural Features for Image Classification. *IEEE Transactions on Systems, Man, and Cybernetics*, SMC-3, 610–621.

39.

Harvey, B.J., Donato, D.C. & Turner, M.G. (2016). Drivers and trends in landscape patterns of stand-replacing fire in forests of the US Northern Rocky Mountains (1984–2010). *Landscape Ecology*, 31, 2367–2383.

40.

Hawbaker, T.J., Vanderhoof, M.K., Beal, Y.J., Takacs, J.D., Schmidt, G.L. & Falgout, J.T. *et al.* (2017). Mapping burned areas using dense time-series of Landsat data. *Remote Sensing of Environment*, 198, 504–522.

41.

Holden, Z.A., Morgan, P. & Evans, J.S. (2009). A predictive model of burn severity based on 20-year satellite-inferred burn severity data in a large southwestern US wilderness area. *Forest Ecology and Management*, 258, 2399–2406.

42.

Holling, C.S. (1973). Resilience and Stability of Ecological Systems. *Annual Review of Ecology and Systematics*, 4, 1–23.

43.

Huang, Q., Swatantran, A., Dubayah, R. & Goetz, S.J. (2014). The influence of vegetation height heterogeneity on forest and woodland bird species richness across the United States. *PLoS ONE*, 9.

44.

Key, C.H. & Benson, N.C. (2006). Landscape assessment: Sampling and analysis methods. *USDA Forest Service General Technical Report RMRS-GTR-164-CD*, 1–55.

45.

Kéfi, S., Guttal, V., Brock, W.A., Carpenter, S.R., Ellison, A.M. & Livina, V.N. *et al.* (2014). Early warning signals of ecological transitions: Methods for spatial patterns. *PLoS ONE*, 9, 10–13.

46.

Kolden, C.A., Smith, A.M.S. & Abatzoglou, J.T. (2015). Limitations and utilisation of Monitoring Trends in Burn Severity products for assessing wildfire severity in the USA. *International Journal of Wildland Fire*, 24, 1023–1028.

47.

Kotliar, N.B. & Wiens, J. a. (1990). Multiple Scales of Patchiness and Patch Structure: A Hierarchical Framework for the Study of Heterogeneity. *Oikos*, 59, 253–260.

48.

Larson, A.J. & Churchill, D. (2012). Tree spatial patterns in fire-frequent forests of western North America, including mechanisms of pattern formation and implications for designing fuel reduction and restoration treatments. *Forest Ecology and Management*, 267, 74–92.

49.

Lenoir, J., Graae, B.J., Aarrestad, P.A., Alsos, I.G., Armbruster, W.S. & Austrheim, G. *et al.* (2013). Local temperatures inferred from plant communities suggest strong spatial buffering of climate warming across Northern Europe. *Global Change Biology*, 19, 1470–1481.

50.

Malone, S.L., Fornwalt, P.J., Battaglia, M.A., Chambers, M.E., Iniguez, J.M. & Sieg, C.H. (2018). Mixed-severity fire fosters heterogeneous spatial patterns of conifer regeneration in a dry conifer forest. *Forests*, 9.

51.

Masek, J.G., Vermote, E.F., Saleous, N.E., Wolfe, R., Hall, F.G. & Huemmrich, K.F. *et al.* (2006). A Landsat Surface Reflectance Dataset. *IEEE Geoscience and Remote Sensing Letters*, 3, 68–72.

52.

McCune, B. (2007). Improved estimates of incident radiation and heat load using non-parametric regression against topographic variables. *Journal of Vegetation Science*, 18, 751–754.

53.

McCune, B. & Keon, D. (2002). Equations for potential annual direct incident radiation and heat load. *Journal of Vegetation Science*, 13, 603–606.

54.

Millar, C.I. & Stephenson, N.L. (2015). Temperate forest health in an era of emerging megadisturbance. *Science*, 349, 823–826.

55.

Miller, J.D., Knapp, E.E., Key, C.H., Skinner, C.N., Isbell, C.J. & Creasy, R.M. *et al.* (2009). Calibration and validation of the relative differenced Normalized Burn Ratio (RdNBR) to three measures of fire severity in the Sierra Nevada and Klamath Mountains, California, USA. *Remote Sensing of Environment*, 113, 645–656.

56.

Miller, J.D. & Thode, A.E. (2007). Quantifying burn severity in a heterogeneous landscape with a relative version of the delta Normalized Burn Ratio (dNBR). *Remote Sensing of Environment*, 109, 66–80.

57.

Moritz, M.A., Morais, M.E., Summerell, L.A., Carlson, J.M. & Doyle, J. (2005). Wildfires, complexity, and highly optimized tolerance. *Proceedings of the National Academy of Sciences*, 102, 17912–7.

58.

Näsi, R., Honkavaara, E., Lyytikäinen-Saarenmaa, P., Blomqvist, M., Litkey, P. & Hakala, T. *et al.* (2015). Using UAV-based photogrammetry and hyperspectral imaging for mapping bark beetle damage at tree-level. *Remote Sensing*, 7, 15467–15493.

59.

North, M.P., Stephens, S.L., Collins, B.M., Agee, J.K., Aplet, G. & Franklin, J.F. *et al.* (2015). Reform forest fire managment. *Science*, 349, 1280–1281.

60.

North, M., Stine, P., Hara, K.O., Zielinski, W. & Stephens, S. (2009). An Ecosystem Management Strategy for Sierran Mixed- Conifer Forests. *General Technical Report PSW-GTR-220*, 1–49.

61.

Park Williams, A., Allen, C.D., Macalady, A.K., Griffin, D., Woodhouse, C.A. & Meko, D.M. *et al.* (2012). Temperature as a potent driver of regional forest drought stress and tree mortality. *Nature Climate Change*, 3, 292–297.

62.

Parks, S.A., Dillon, G.K. & Miller, C. (2014). A new metric for quantifying burn severity: The relativized burn ratio. *Remote Sensing*, 6, 1827–1844.

63.

Prichard, S.J. & Kennedy, M.C. (2014). Fuel treatments and landform modify landscape patterns of burn severity in an extreme fire event. *Ecological Applications*, 24, 571–590.

64.

Questad, E.J. & Foster, B.L. (2008). Coexistence through spatio-temporal heterogeneity and species sorting in grassland plant communities. *Ecology Letters*, 11, 717–726.

65.

R Core Team. (2018). *R: A language and environment for statistical computing. http://www.r-project.org/*. R Foundation for Statistical Computing, Vienna, Austria.

66.

Raffa, K.F., Aukema, B., Bentz, B.J., Carroll, A., Erbilgin, N. & Herms, D.A. *et al.* (2009). A literal use of 'forest health' safeguards against misuse and misapplication. *Journal of Forestry*, 276–277.

67.

Raffa, K.F., Aukema, B.H., Bentz, B.J., Carroll, A.L., Hicke, J.A. & Turner, M.G. *et al.* (2008). Cross-scale drivers of natural disturbances prone to anthropogenic amplification: The dynamics of bark beetle eruptions. *BioScience*, 58, 501.

68.

Reilly, M.J., Dunn, C.J., Meigs, G.W., Spies, T.A., Kennedy, R.E. & Bailey, J.D. *et al.* (2017). Contemporary patterns of fire extent and severity in forests of the Pacific Northwest, USA (1985-2010). *Ecosphere*, 8.

69.

Reusch, T.B.H., Ehlers, A., Hämmerli, A. & Worm, B. (2005). Ecosystem recovery after climatic extremes enhanced by genotypic diversity. *Proceedings of the National Academy of Sciences*, 102, 2826–2831.

70.

Rouse, J.W., Hass, R.H., Schell, J. & Deering, D. (1973). Monitoring vegetation systems in the great plains with ERTS. *Third Earth Resources Technology Satellite (ERTS) symposium*, 1, 309–317.

71.

Scholl, A.E. & Taylor, A.H. (2010). Fire regimes, forest change, and self-organization in an old-growth mixed-conifer forest, Yosemite National Park, USA. *Ecological Applications*, 20, 362–380.

72.

Sikkink, P.G., Dillon, G.K., Keane, R.E., Morgan, P., Karau, E.C. & Holden, Z.A. *et al.* (2013). *Composite Burn Index (CBI) data and field photos collected for the FIRESEV project, western United States*. Forest Service Research Data Archive, Fort Collins, CO.

73.

Steel, Z.L., Safford, H.D. & Viers, J.H. (2015). The fire frequency-severity relationship and the legacy of fire suppression in California forests. *Ecosphere*, 6, 1–23.

74.

Stein, A., Gerstner, K. & Kreft, H. (2014). Environmental heterogeneity as a universal driver of species richness across taxa, biomes and spatial scales. *Ecology Letters*, 17, 866–880.

75.

Stephens, S.L. & Collins, B.M. (2004). Fire regimes of mixed conifer forests in the North-Central Sierra Nevada at multiple scales. *Northwest Science*, 78, 12–23.

76.

Stephens, S.L., Fry, D.L. & Franco-Vizcaíno, E. (2008). Wildfire and spatial patterns in forests in northwestern

Mexico: The United States wishes it had similar fire problems. *Ecology and Society*.

77.

Stephens, S.L., Lydersen, J.M., Collins, B.M., Fry, D.L. & Meyer, M.D. (2015). Historical and current landscape-scale ponderosa pine and mixed conifer forest structure in the Southern Sierra Nevada. *Ecosphere*, 6, 1–63.

78.

Stephens, S.L., Moghaddas, J.J., Edminster, C., Fiedler, C.E., Haase, S. & Harrington, M. *et al.* (2013). Fire Treatment Effects on Vegetation Structure, Fuels, and Potential Fire Severity in Western U. S. Forests. *Ecological Applications*, 19, 305–320.

79.

Sugihara, N.G. & Barbour, M.G. (2006). Fire and California vegetation. In: *Fire in california's ecosystems* (eds. Sugihara, N.G., Van Wagtendonk, J.W., Shaffer, K.E., Fites-Kaufman, J. & Thode, A.E.). University of California Press, Berkeley; Los Angeles, CA, USA, pp. 1–9.

80.

Tilman, D. (1994). Competition and biodiversity in spatially structured habitats. *Ecology*, 75, 2–16.

81.

Trumbore, S., Brando, P. & Hartmann, H. (2015). Forest health and global change. *Science*, 349.

82.

Tuanmu, M.-N. & Jetz, W. (2015). A global, remote sensing-based characterization of terrestrial habitat heterogeneity for biodiversity and ecosystem modelling. *Global Ecology and Biogeography*, n/a–n/a.

83.

USGS. (2017a). Product Guide: Landat 8 Surface Reflectance Code (LaSRC) Product. *USGS Professional Paper*, 4.2.

84.

USGS. (2017b). Product Guide: Landsat 4-7 Surface Reflectance (LEDAPS) Product. *USGS Professional Paper*, 8, 38.

85.

Veraverbeke, S. & Hook, S.J. (2013). Evaluating spectral indices and spectral mixture analysis for assessing fire severity, combustion completeness and carbon emissions. *International Journal of Wildland Fire*, 22, 707–720.

86.

Vermote, E., Justice, C., Claverie, M. & Franch, B. (2016). Preliminary analysis of the performance of the Landsat 8/OLI land surface reflectance product. *Remote Sensing of Environment*, 185, 46–56.

87.

Virah-Sawmy, M., Willis, K.J. & Gillson, L. (2009). Threshold response of Madagascar's littoral forest to sea-level rise. *Global Ecology and Biogeography*, 18, 98–110.

88.

Walker, B., Holling, C.S., Carpenter, S.R. & Kinzig, A. (2004). Resilience, adaptability, and transformability in social-ecological systems. *Ecology and Society*, 9, 5.

89.

Westerling, A.L. (2016). Increasing western US forest wildfire activity: Sensitivity to changes in the timing of spring. *Philosophical Transactions of the Royal Society B: Biological Sciences*, 371, 20160373.

90.

Westerling, A.L., Hidalgo, H.G., Cayan, D.R. & Swetnam, T.W. (2006). Warming and earlier spring increase western U.S. forest wildfire activity. *Science*, 313, 940–943.

91.

Wood, E.M., Pidgeon, A.M., Radeloff, V.C. & Keuler, N.S. (2012). Image texture as a remotely sensed measure of vegetation structure. *Remote Sensing of Environment*, 121, 516–526.

92.

Young, D.J.N., Stevens, J.T., Earles, J.M., Moore, J., Ellis, A. & Jirka, A.L. *et al.* (2017). Long-term climate and competition explain forest mortality patterns under extreme drought. *Ecology Letters*, 20, 78–86.

93.

Zhu, Z., Key, C., Ohlen, D. & Benson, N. (2006). Evaluate Sensitivities of Burn-Severity Mapping Algorithms for Different Ecosystems and Fire Histories in the United States. *Final Report to the Joint Fire Science Program, Project JFSP 01-1-4-12*, 1–35.